Prolonged energy harvesting for ingestible devices

As accepted for publication in

Nature Biomedical Engineering

Title

Prolonged energy harvesting for ingestible devices

Authors

Phillip Nadeau[1], Dina El-Damak[1], Dean Glettig[2], Yong Lin Kong[2], Stacy Mo[2], Cody Cleveland[2,3], Lucas Booth[2], Niclas Roxhed[2,4], Robert Langer[2,5,6,*], Anantha P. Chandrakasan[1,*], Giovanni Traverso[2,3,*]

Affiliations

[1] Department of Electrical Engineering and Computer Science, and the Microsystems Technology Laboratories, Massachusetts Institute of Technology, Cambridge, Massachusetts 02139, USA

[2] Department of Chemical Engineering and Koch Institute for Integrative Cancer Research, Massachusetts Institute of Technology, Cambridge, Massachusetts 02139, USA.

[3] Division of Gastroenterology, Brigham and Women's Hospital, Harvard Medical School, Boston, MA 02115

[4] Department of Micro and Nanosystems, KTH Royal Institute of Technology, 10044 Stockholm, Sweden

[5] Media Lab, Massachusetts Institute of Technology, Cambridge, Massachusetts 02139, USA

[6] Institute for Medical Engineering and Science, Massachusetts Institute of Technology, Cambridge, Massachusetts 02139, USA

Contact information

*To whom correspondence may be addressed. Email: ctraverso@partners.org, rlanger@mit.edu and anantha@mtl.mit.edu

Abstract

Ingestible electronics have revolutionized the standard of care for a variety of health conditions. Extending the capacity and safety of these devices, and reducing the costs of powering them, could enable broad deployment of prolonged monitoring systems for patients. Although previous biocompatible power harvesting systems for in vivo use have demonstrated short (minute-long) bursts of power from the stomach, little is known about the capacity to power electronics in the longer term and throughout the gastrointestinal tract. Here, we report the design and operation of an energy-harvesting galvanic cell for continuous in vivo temperature sensing and wireless communication. The device delivered an average power of 0.23 μW per mm^2 of electrode area for an average of 6.1 days of temperature measurements in the gastrointestinal tract of pigs. This power-harvesting cell has the capacity to provide power for prolonged periods of time to the next generation of ingestible electronic devices located in the gastrointestinal tract.

Thanks to recent advances in ingestible electronics, it is now possible to perform video capture[1], electronically-controlled drug release[2], pH, temperature, and pressure recording[3], and heart rate and respiration monitoring[4], all from within electronic pill-like capsules placed in the gastrointestinal (GI) tract. Recent progress in energy harvesting and wireless power transfer is offering new options to power these devices, but many are not well suited to ingestible capsules. For example, traditional harvesting sources such as thermal[5], and vibration[6] energy harvesting are complicated by the lack of thermal gradients in the stomach and challenges in obtaining mechanical coupling to motion sources. Wireless power-transfer via near-field[7] or mid-field[8] coupling is also challenging in this case, due to the unconstrained position and orientation of the capsule. Hence, there is still a strong reliance on primary cell batteries for ingestible electronics. Hence, most current ingestible electronics still rely on primary cell batteries, many of which require toxic materials, have limited shelf life due to self-discharge and can cause mucosal injury[9]. There is therefore a need to explore alternative sources, particularly as the circuits scale to lower average power, to enable their use in a practical system.

A few key trends have led to our work. For one, the average power demands of Complementary Metal-Oxide-Semiconductor (CMOS) technology have been scaling into the nanowatt (nW) level thanks to advanced design techniques and technology improvements[10–12], enabling a wider array of harvesters. Next, advances in material design and packaging have demonstrated fully passive gastric devices that are small enough to be swallowed, but then unfold after ingestion to remain long term, up to 7 days in the stomach for ultra-long drug delivery[13]. Such devices could one day provide an ingestible non-invasive platform for active wireless electronic sensors that perform long term *in vivo* vital signs monitoring. Finally, interest in bio-compatible galvanic cells is rising, with a focus on (1) transient electronics that fully disappear at the end of their tasks[14], (2) electrolytes that are supplied on demand to extend the shelf life of the cell[15], (3) material selection for fully biocompatible and

biodegradable cells[14–17] and recently, (4) edible gastric-Mg-Cu cells, which can power near-field communication of medication compliance information to a body-worn patch for up to a few minutes[18]. Additional support for the potential of long-term harvesting is provided by two in vitro studies on cells in synthetic gastric-fluid- like electrolytes, which demonstrated measurements lasting a number of hours[19,20].

This has led us to investigate the practical use of a biocompatible galvanic cell for powering a wireless sensor node in the GI tract. Here, we report an energy-harvesting system with temperature sensing and wireless communication, evaluated in a porcine model. We demonstrate a fully autonomous sensor system, created from commercial semiconductor parts, and powered solely by the cell and capable of providing central temperature measurements. The device can also use the harvested power to activate drug release via electrochemical dissolution of a gold membrane.

Results

Basic principle and initial characterization

The bio-galvanic cell characterized in this work consists of a redox couple formed by a dissolving metallic anode that undergoes galvanic oxidation and an inert cathode that returns electrons to the solution. In our case, the gastric or intestinal fluids of the surrounding environment form the electrolyte. The final performance of the cell is a strong function of environmental conditions that change significantly during normal gastrointestinal routines. For example, the pH, chemical composition, and heterogeneity of the stomach contents[21] vary considerably throughout the day. Hence there is a need to obtain the performance of the cell directly by *in vivo* measurement characterization. As previous studies have noted[14,22], the cathodic reaction proceeds with either hydrogen gas evolution

or by the reduction of dissolved oxygen gas depending on the pH of the solution, and is usually limited by mass-transport conditions. The relevant cathodic reactions are given by:

$$2\,H^{+} + 2\,e^{-} \leftrightarrow H_2 \quad (1)$$

$$O_2 + 2H_2O + 4e^{-} \leftrightarrow 4OH^{-} \quad (2)$$

A number of materials have been proposed as dissolving anodes, most prominently, magnesium[18,23] and zinc[15,19,20], which are noted for their dietary value[24], low cost, ease of manufacturability, and their relatively low position in the electrochemical series[25]. The reaction at the anode is given by:

$$X \leftrightarrow X^{n+} + n\,e^{-} \quad (3)$$

where X = Mg or Zn. The cathode, which sends electrons back into the solution, was created from pure copper metal[26].

Given prior successes in utilizing magnesium, which has a higher reduction potential, for in vivo power generation[18], we first considered magnesium anodes for our initial *in vivo* characterization evaluating the impact of electrode size. In Figure 1 (a)-(d), we characterized a Mg-Cu electrode system in a porcine model using small square electrodes of differing areas, mounted on the tip of an endoscope as shown in Fig. 1(a) (see *Methods*). The current density was stepped in fixed increments resulting in the voltage and power densities shown in Fig 1(b). The resulting average peak power density across all sizes shown in Fig 1(c) was 2.48 $\mu W/mm^2$ in the stomach (0.97 $\mu W/mm^2$ in the duodenum), and the average observed cell voltage in Fig 1(d) was 0.23 V. Consistent with the low observed cell voltage, we also noted a large amount of corrosion on the magnesium electrodes, suggesting that the lifetime of a magnesium-based prototype would not exceed 24 h, thereby making week-long wireless measurements unfeasible.

Motivated by the observations of corrosion and given the intention to evaluate extended gastric residence of these electrodes, we performed extended *in vitro* studies of electrode longevity (see *Methods*). With the configuration shown in Fig 1(e), we compared Mg and Zn anodes in side-by-side measurements using a load-sweep methodology (50 kΩ down to 150 Ω in 255 steps). Fig 1(f) shows the maximum power observed in each load resistance sweep. The Mg anode gave 1.3× higher cell voltage and 6× higher peak power density, but the Zn anode lasted much longer (more than 23×), suggesting Zn for longer term use. The combination of the experiments presented in Figure 1 allowed us to proceed to the design of a zinc-based measurement capsule to enable evaluation of the power parameters via a stand-alone device *in vivo*.

Characterization in the stomach environment

We created a measurement capsule (Figure 2, and Methods) to obtain detailed measurements of the performance of the Zn-Cu cell in a porcine stomach and transmit the results to a nearby basestation. The design was fully self-sufficient and wireless to avoid a tether to the outside that could reduce the practical measurement duration or impact the comfort or normal routines of the animal. A conventional coin-cell battery powered the capsule in order to avoid loading the electrodes with the demands of the circuitry during measurement, allowing a precise characterization of the cell with a separate controllable load.

The capsule was created using all commercial low-cost semiconductor parts (Fig. 2 a and b) and consisted of: (1) an 8-bit digitally controlled potentiometer[27] to set the load resistance of the cell, and (2) a microcontroller system-on-chip[28] and its associated peripherals, which contained (i) a 10-bit analog-to-digital converter (ADC) that measured the electrode voltage, (ii) a temperature sensor, (iii) a wireless transmitter, and (iv) a processor that ran software code to control all of the functions.

To characterize the cell, the software was programmed sweep the load resistance through all 256 available codes (50 kΩ down to 150 Ω in 255 linear steps), taking voltage measurements at each point. Each step was held for 2 s, and at the end of a sweep, the resistor was reset to 50 kΩ and held for a further 64 s for the electrode voltage to re-equilibrate to the light-load condition before starting the next measurement (full measurement time: 576 s per sweep). The data, which included electrode voltages at each of the 256 resistor-codes, and the temperature sensor measurements, were transmitted as a Frequency-Shift-Keying-modulated, +10 dBm, 920 MHz wireless signal, to a commercial basestation receiver, mounted about 2 m away (resistance sweep methodology flow diagram and example measured waveforms illustrated in Supplementary Fig. 1 and 2 respectively). We also characterized the Zn-Cu cell and measurement electronics in synthetic gastric fluid (SGF) *in vitro* prior to the animal experiments (data shown in Supplementary Fig. 3).

The measurement capsule was initially deployed in five animals with the results summarized in Fig. 2(d)-(i) and full data shown in Supplementary Fig. 4 and 5 (see *Methods* for experimental details). Due to the recognized slow motility of the porcine GI tract[29,30] and the size of the capsule, the devices were retained in the animal for 7 days to 10 days without additional design considerations. During this time, the data were collected as the animal performed its normal daily routines. The traces in Fig. 2(d)-(f) correspond to an example device, and show the electrode voltage measured at the point of maximum power density for each load resistance sweep (one sample every 576 s), as well as the associated peak power density level, and the temperature recorded by the temperature sensor. Figs. 2(h) and 2(i) give the statistics of the measured peak power and optimum source voltage. Across all five stomach-deployed capsules, the mean time for which power was available, the mean peak power P_{max}, and mean voltage at P_{max} were 5.0 days, 1.14 $\mu W/mm^2$ and 0.149 V respectively. There was a large amount of

variation in the transit time of the devices, which was anticipated and consistent with prior observations of the porcine GI tract[29–31].

Interestingly, by correlating the anatomic location of the capsule determined through serial x-rays we demonstrated that the peak power drops significantly after passage through the pylorus to the small intestine. The combination of Figs. 2(e) and 2(g) shows an example of this correlation. To confirm this observation, we deployed 3 devices directly into the small intestine and tracked their passage through the colon until exit. The three devices showed an average of 13.2 nW/mm^2 of peak power density and the power remained present, between 1 to 100 nW/mm^2, throughout the passage time until exit (see Supplementary Fig. 4).

Harnessing power in vivo for sensing, communication, and drug delivery

To demonstrate the utility of the energy obtained, we created a second capsule powered entirely by the Zn-Cu cell (see Figure 3, and *Methods*). This harvested power was used for all functions of the capsule, which included temperature measurement, software control, and wireless transmission to a basestation located 2 m away. In this design (Fig. 3a) we used a commercial energy harvesting boost-converter integrated circuit (IC)[32], which took energy directly from the Zn-Cu cell at low voltage (0.1 to 0.2 V) and boosted it onto a temporary storage capacitor at a higher voltage (between 2.2 and 3.3 V) for use by the circuits. The encapsulated sensor device prepared for deployment is shown in Fig 3(b).

When the input source is applied, the boost converter IC pulls energy from the input voltage V_{in} and transitions through a startup region. Once the startup is complete, the main higher-efficiency boost converter is activated and sets the OK signal, which then powers the microcontroller through a switch. From here the microcontroller transmits packets containing temperature measurement data at a variable rate depending on the input power. Fig. 3(c) shows an example of steady state operation of the capsule,

where the storage capacitor is slowly charged until enough energy is available for packet transmission. The system regulates the rate by periodically sampling the supply voltage V_{DD} to determine whether to send a packet or wait for more energy to be harvested. If the sampled voltage is below 3.0 V, the system remains in a low-energy sleep mode for 4 s before attempting to sample again. If the voltage is above 3.0 V, the system transmits a packet and then returns to periodically sampling the voltage (initially 0.5 s after the packet, and then again every 4 s) to determine when to transmit the next packet. Further details on the capsule design and operation are provided in Supplementary Figs. 6, 7, and 8.

Since packet transmission is the dominant energy consumer, we used the number of transmitted packets in a given window length (t_{window}) to estimate the overall amount of energy delivered to the load. Each packet is 176 bits long including preamble and headers and is transmitted at 50 kbps, resulting in a 3.5 ms packet transmitted at +10 dBm. Prior to the experiments, a laboratory source-meter was used to characterize the energy consumed by the capsule in transmitting each packet as a function of the V_{DD}, $E_{pkt} = f(V_{DD})$. Then during the *in vivo* experiment, the number of packets transmitted during a given interval was used to determine the average power ($P_{sys,avg}$) delivered to the load using:

$$P_{sys,avg} = \frac{1}{t_{window}} \sum_{all\ m} E_{pkt}(V_{DD}[m]) \qquad (4)$$

where m represents a packet and Σ is the sum over all the packets transmitted within t_{window}. $V_{DD}[m]$ is the measured system V_{DD} at the beginning of each packet transmission – information that was transmitted along with the temperature measurement data. To obtain an accurate packet count despite the possibility of dropped packets, we also transmit an internally generated packet count to the basestation along with the other measurements.

The system was deployed in 3 animals and the results are summarized in Fig. 3(d) (full measurements in Supplementary Fig. 9). Fig 3(e) shows the power delivered from the cell to the load using eqn. (3), with $t_{window} = 1$ h. Fig 3(f) shows the measured temperature sensor data, and Fig 3(g) shows the RF signal strength seen by the receiving basestation for each packet. Of note was that temperature readings below the expected core or central temperature were observed to coincide with daytime hours and times around feeding (Fig. 3f), probably representing transient temperature decrement associated with ingestion of foods and liquids. The disconnected regions in the figures represent periods for which electrical power was not sufficient to send wireless packets, for example, due to variations in both the fluidic environment of the stomach and the position of the capsule within it. On average, packets were received in 91% of the 1 h time slots during the three experiments. Across all of the experiments, the devices operated for a mean of 6.1 days, delivering an average power of 0.23 μW per mm^2 of electrode area to the load, and transmitting packets with temperature measurements every 12 seconds.

To further demonstrate the utility of the energy harvested by the system, we designed and fabricated a device for drug release that can be triggered with the harvested energy, as shown in Fig 3(h), and tested this device *in vitro* with physiologic gastric fluid (See *Methods* for the details of device fabrication). The device, as shown in Fig 3(i), encapsulates a model drug (in this case, methylene blue) in a PMMA reservoir (2 mm × 1 mm × 1.5 mm) that is sealed with a 300 nm thick gold membrane. The release is achieved via electrochemical dissolution of the membrane, as demonstrated previously by Santini et. al[33]. The gold membrane, which is otherwise inert in the gastric environment, can be chemically corroded when the potential is raised (+1.04 V with respect to Saturated Calomel Electrode) to allow formation of water-soluble chloro-gold complexes[34]. Our results show that the device remains intact when it is connected to the system ground (shorted to the zinc electrode) in physiologic gastric

fluid (See *Methods* for experimental details). Upon activation via the application of discharge of voltage from 2.0 to 2.3 V with respect to zinc system ground, the corrosion of the gold weakens the membrane integrity, causing crack formation that is visible at t = 155 minutes (blue arrow, shown in the middle inset of Fig. 3j), and ultimately the visible release of the contents (indicated with red arrow at the right inset of Fig. 3j.) through the corroded membrane. The voltage profile plotted in Fig 3(k) shows the discharge characteristics that gradually activate the release. The initial shallow ramp from 3.15 V to 2.95 V represents the microcontroller boot-up followed by temperature measurement. The steep drop from 2.95 V to 2.3 V represents the packet transmission, and the more slow discharge from 2.3 V to 2.0 V represents charges delivered to the gold electrode. With the 220 μF storage capacitance, this represents 66 μC of charge delivered to the electrode per pulse. The pulse ends when the boost converter toggles the OK signal to low (due the storage voltage declining below the threshold), which deactivates the microcontroller and release electrode switch, and allows the storage capacitor to begin charging in preparation for the next cycle. The average pulse interval during the experiment was 11.9s, and charge delivery rate was 5.5 μC/s. For the designed size of 2 mm x 1 mm active gold area (with 300 nm thickness), the total theoretical charge necessary to completely dissolve the electrode was 17.0 mC, and hence an ideal dissolution time of 51 min. In gastric fluid, it is expected that side reactions can occur on the electrode surface resulting in a longer release time, hence the observed time of 155 min.

Discussion

Ingestible electronics have an expanding role in the evaluation of patients[35]. The potential of applying electronics or electrical signals for treatment is being explored[36] and the potential for long term monitoring and treatment is being realized through the development of systems with the capacity for safe extended gastrointestinal residence[13,37]. Energy alternatives for GI systems are needed to enable broad applicability, especially given size and biocompatibility constraints coupled with the potential need for long-term power sources and low cost systems.

Here we report the *in vivo* characterization of a galvanic cell composed of inexpensive biocompatible materials, which are activated by GI fluid. We have demonstrated energy harvesting from the cell for up to 6 days (average power 0.23 $\mu W/mm^2$) and using this energy we have developed a self-powered device with the capacity for central temperature measurement and wireless transmission from within a large animal model. The combining of the cell with a boost converter in the energy harvesting IC allowed the system to power these more complex electronics, even as the cell voltage and power level varied during the experiments.

The device we have fabricated could be rapidly implemented for the evaluation of core body temperature and for the evaluation of GI transit time given the differential temperature between the body and the external environment. A recent study evaluating data collected from 8682 patients found that peripheral temperature readings did not have acceptable clinical accuracy to guide clinical decisions[38]. Hence, continuous automated central temperature measurements via a wireless ingestible system may provide significant clinical benefit. We have also demonstrated, via a custom designed drug release device, that such an energy harvesting method could be used to activate drug delivery via a gold membrane corrosion mechanism. This proof of concept could ultimately allow the incorporation drug delivery in the ingestible electronic capsule.

Furthermore, we have characterized and demonstrated the capacity for harvesting from across the GI tract including stomach, small intestine and colon. Interestingly, the available power density ranged between a few $\mu W/mm^2$ down to a few nW/mm^2 across the GI tract. The reduced power in the intestine could potentially be explained by anatomical variation between it and the stomach -- diffusion could be impaired by close contact with the intestinal walls. Further development will be required to delineate the exact causes and could lead to an improved design. In the meantime, these observations may guide future development of gastrointestinal resident electronic power harvesting systems according to their targeted anatomic location. For example, there may be a need for greater storage capability to carry energy from the stomach, or depending on the application, it may be necessary to support even lower power modes.

Our electrode area in this study was limited by the availability of a nanowatt-level commercial harvester. Nevertheless, the total elemental zinc present in our largest tested electrode (30 mm x 3.0 mm x 0.25 mm) was 161 mg. Assuming extreme case of full dissolution across the six-day experiment, the average zinc ion deposit rate for this electrode would be 27 mg/day. This amount is below the US Food and Nutrition Board recommended upper limit UL = 40 mg/day[24], and in line with levels found in over-the-counter zinc supplements (15, 30, and 50 mg/day dosings are commonly available). Looking ahead, we would expect that a custom designed system would be able to target much lower power levels and hence integrate smaller electrodes and less zinc deposition than we have tested here.

Research in ultra-low-power electronics continues to push the boundaries of the average power consumption, and already provides a range of options for circuits that could be adapted for use in GI applications at the nanowatt level. Examples include energy harvesters (for < 10 nW available power[10–12]), ADCs and signal acquisition circuits (< 10 nW[39,40]), far field wireless transmitters (< 1 nW standby[41]), and mm-scale sensor nodes with sensing and processing (< nW standby[42]). Such systems

could allow the electrode dimensions to scale to just a millimetre or two in width and length, and could enable broad applications for extended power harvesting from alternative cells for long term monitoring of vital signs[4] and other parameters in the GI tract, especially with the introduction of devices that are deployed endoscopically[43] or self-administered[13] and have the capacity to reside in the gastric cavity for prolonged periods of time.

Though sufficient for our animal studies, one limitation is the size of the capsule. Without a clear picture of the expected voltage and power levels *in vivo* at the outset, achieving further miniaturization as part of this study would have been challenging. Given our measured results, and with further engineering development, for example, to create a custom single-chip Application Specific Integrated Circuit (ASIC) and to apply enhanced packaging techniques like component stacking, the design could potentially be miniaturized by 3 to 5× as compared to the volume of the currently presented hardware. In addition, future work should strive to match animal behavior information, such as feeding and motion data, with the measured power level and observed physiologic signals in order to better understand the sources of variations observed here.

One further limitation is the physical design of the electrochemical cell. Our focus was on powering robust *in vivo* measurements over longer periods of time compared to previously reported cells. However, future work should include efforts to improve the voltage and power of the cell; for example, by integrating membranes to improve proton exchange[20] while controlling corrosion of the electrodes[44]. In addition, further improving the efficiency of low-voltage boost converters at ultra-low power levels will facilitate demonstration with smaller electrode areas (approaching 1 mm x 1 mm), or allow energy harvesting across the entire GI tract. Another important direction of future research will be the development of systems that can be safely retained in the GI tract over long periods, thereby enabling self-powered monitoring on the order of weeks, months or even years following a single

ingestion. This work should focus on solving material-, packaging-, and interface-related challenges in order to design a capsule for eventual human trials.

Methods

Magnesium, zinc and copper electrode fabrication and attachment. All electrodes were created from pure metal foils (Alfa Aesar, 0.25 mm thick) and cut to the specified length and width dimensions to within ± 10%. Attachment of the zinc and copper electrodes to wires or to the PCBs was performed with standard solder and flux, whereas magnesium, which is not solderable, was attached with 2-part silver conductive epoxy (8331, MG Chemicals).

In vivo characterization of magnesium-copper system. Electrodes (with attached wires) were fixed via thermoplastic adhesive to opposite sides of a 3D-printed post (30 mm long, 3.8 mm diameter) for easy mounting on an endoscope for guidance into the stomach and duodenum. The electrodes were connected by a ~3m long cable which passed through the lumen of the endoscope to a Keithley 6430 source-meter, which executed the specified current steps and voltage measurements from outside the animal.

Electrode longevity comparison. Electrode anode and cathode (with attached wires) were placed side-by-side (3 mm separation) on a polystyrene support and fixed using 2-part epoxy (20845, Devcon), with 10 mm electrode length exposed. The electrode pairs were submerged in a pH 4 buffer solution (33643, Fluka Analytical) and measured using the same electronics as the characterization capsule, described below.

Characterization and demonstration capsule fabrication: The PCBs for the capsules were 4-layer FR4, with 35-µm copper metallization. The electrodes were soldered onto the PCB for protrusion outside the encapsulation. Encapsulation was performed as a 2-step process. Prior to

polydimethylsiloxane (PDMS) moulding, the boards were fully coated in 2-part epoxy (1-2 mm thick) to act as sealant against moisture and prevent fluid from entering the device via the protruding electrodes. The outer layer was PDMS (Sylgard 184, Dow Corning), selected for biocompatibility with the stomach environment and moulded into a capsule shape to facilitate passage through the GI tract. The electrodes protruded through the back of the encapsulated device and were bent around towards the front and secured to the outer layer of the PDMS with 2-part epoxy (20845, Devcon).

In vivo characterization. All procedures were conducted in accordance with the protocols approved by the Massachusetts Institute of Technology Committee on Animal Care. In vivo porcine studies were performed in female Yorkshire pigs aged between 4 and 8 months and weighing approximately 45-50 kg. The porcine model was specifically selected given prior observations noting slower transit time and thereby providing the capacity for extended residence of a macroscopic device in the GI tract[29,30]. Animal sample size was guided by prior work demonstrating proof-of-concept studies with gastrointestinal drug delivery and sensor systems[4,13,45]. In vivo experiments were not blinded or randomized. Prior to endoscopy or administration of the prototypes the animals were placed on a liquid diet for 48 hours. The animals were fasted overnight immediately prior to the procedure. On the day of the procedure for the endoscopic characterization studies the animals received induction of anesthesia with intramuscular injections of Telazol (tiletamine/zolazepam) 5 mg/kg, xylazine 2 mg/kg, and atropine (0.04 mg/kg), the pigs were intubated and maintained on inhaled isoflurane 1-3%. For the deployment of the capsule prototypes the animals were sedated via intramuscular injections of the above agents. The esophagus was intubated and an esophageal overtube placed (US Endoscopy). The prototypes were delivered directly to the gastric cavity or endoscopically placed in the small intestine through the overtube. Prototypes were followed with serial x-rays. A total of five stomach-deposited

characterization devices were evaluated in five separate pig experiments. One device (C1) was retrieved early from the small intestine after recording for 8.3d and passing through the pylorus. Two devices stopped their recording early owing to leakages in the PDMS/epoxy encapsulation: one after 7.1 days of measurement but prior to reaching the small intestine (C2), and one after 10.1 days of measurement, including 8.0 days in the stomach and 2.1 days spent in the small intestine (C4), as estimated by the observed power density drop. Two devices (C3 and C5) recorded all the way to exit (8.8d and 7.5d of recording). The four devices reaching the small intestine exhibited significant power density drops co-inciding with extra gastric location. Three additional characterization devices (C6 to C8) were deployed directly into the duodenum to confirm the power density differential, all of which recorded from deposition until exit (3.0d, 2.9d, and 2.3d respectively). Finally, three self-powered temperature devices (D1 to D3) were evaluated in three separate pig experiments (6.8d, 6.6d, and 4.7d respectively). All three self-powered devices were deployed in the gastric cavity. Before placing the devices, the electrodes were temporarily supplied with 3 V from an external source in order to guarantee cold-start of the harvester and to obtain a temperature reading from the room for offline calibration of the temperature measurement data. During and after the experiment, we did not see evidence of toxicity from clinical observation. While in place animals were maintained on a liberalized diet.

Drug release prototype fabrication. Drug cavities and the substrate of the release prototype were first defined with a conventional carbon dioxide laser engraver (Universal Laser Systems VLS 6.60, Engraving Systems LLC) on a 1.5 mm thick poly(methyl methacrylate) (PMMA) board (KJ-35052050, McMasterCarr). A 300 nm thick gold layer was deposited on a separate PMMA substrate using an electron beam evaporator and a polyvinyl alcohol (PVA) film was adhered to the gold surface. The

gold/PVA layer was then peeled off from the substrate and transferred to the delivery device to seal the cavity by stamping the device into a thin layer of low viscosity epoxy (EPO-TEK 301-1, Epoxy Technology). Here the PVA film acts as a dissolvable temporary support layer to provide mechanical rigidity for the 300 nm thin gold film during the transfer process. Methylene blue (M9140, Sigma Aldrich) is then added to the reservoir, accessible from the bottom of the device, before it is sealed with high viscosity epoxy (20445, Devcon). The relatively high viscosity prevents the infiltration of the sealant to the filled cavity. Following curing of the epoxy, the sealed device was put into DI water to dissolve the temporary PVA film and subsequently dried in air. An electrical connection was then made to the gold layer using conductive epoxy (CW2400, Circuitworks). Finally, all conductive areas except the membrane portion of the gold layer covering the drug cavity were insulated with medium-viscosity UV-curable epoxy (EPO-TEK OG116-31, Epoxy Technology) and subsequently UV cured.

Demonstration of activated drug release. The release prototype and zinc and copper electrodes (preparation as described earlier with 30 mm length and 3 mm width) were submerged in physiologic gastric fluid. Gastric fluid was endoscopically extracted from live Yorkshire pigs that were on liquid diet two days prior to the procedure. The drug release prototype was connected to a controller board described earlier, which harvests and releases the captured energy to the prototype. The demonstration proceeded in two phases, (1) a control phase, and (2) the release phase. In the control phase, the integrity of the device is first tested submerged in gastric fluid (47 hours in our case), while the potential of the gold membrane was maintained at the system ground (0 V relative to the zinc). Upon determination of its mechanical integrity, and examining the membrane for leakage, the reservoir along with harvesting electrodes were placed in a fresh sample of gastric fluid for the release phase. In this phase, the controller was configured to short the reservoir electrode to the system V_{STOR} to deliver

packets of charge at the end of each wake-up interval in order to corrode the electrode. The device submerged in gastric fluid was observed through a macroscopic lens, and the electrical profile was collected through an oscilloscope.

Data collection: A commercial transceiver evaluation board (SmartRF TrxEB, Texas Instruments) was used to receive the 900 MHz FSK packets transmitted from the capsules. For the large animal experiments, the board and its antenna were mounted above the steel cage area that housed the animals (about 2 m above the ground). The transceiver board was connected via USB cable to a laptop that saved the raw packet information for later offline processing in MATLAB version 2014b (MathWorks).

Code availability: The microcontroller code that was used in this study is available in Figshare with the identifier "doi:10.6084/m9.figshare.4451420"[46]. Certain proprietary code from Microchip Inc. that was used in the microcontroller is not publicly available.

Data availability: The data that support the findings of this study are available in Figshare with the identifier "doi:10.6084/m9.figshare.4451420"[46]. The authors declare that all other data supporting the findings of this study are available within the paper and its Supplementary Information.

References

1. Iddan, G., Meron, G., Glukhovsky, A. & Swain, P. Wireless capsule endoscopy. *Nature* **405,** 417 (2000).
2. van der Schaar, P. J. *et al.* A novel ingestible electronic drug delivery and monitoring device . *Gastrointest. Endosc.* **78,** 520–528 (2013).
3. Maqbool, S., Parkman, H. P. & Friedenberg, F. K. Wireless capsule motility: Comparison of the SmartPill(R) GI monitoring system with scintigraphy for measuring whole gut transit. *Dig. Dis. Sci.* **54,** 2167–2174 (2009).
4. Traverso, G. *et al.* Physiologic Status Monitoring via the Gastrointestinal Tract. *PLoS One* **10,** e0141666–e0141666 (2015).
5. Ramadass, Y. K. & Chandrakasan, A. P. A Battery-Less Thermoelectric Energy Harvesting Interface Circuit With 35 mV Startup Voltage. *IEEE J. Solid-State Circuits* **46,** 333–341 (2011).
6. Dagdeviren, C. *et al.* Conformal piezoelectric energy harvesting and storage from motions of the heart, lung, and diaphragm. *Proc. Natl. Acad. Sci.* **111,** 1927–1932 (2014).
7. Waters, B. H., Sample, A. P., Bonde, P. & Smith, J. R. Powering a Ventricular Assist Device (VAD) With the Free-Range Resonant Electrical Energy Delivery (FREE-D) System. *Proc. IEEE* **100,** 138–149 (2012).
8. Ho, J. S. *et al.* Wireless power transfer to deep-tissue microimplants. *Proc. Natl. Acad. Sci.* **111,** 7974–7979 (2014).
9. Laulicht, B., Traverso, G., Deshpande, V., Langer, R. & Karp, J. M. Simple battery armor to protect against gastrointestinal injury from accidental ingestion. *Proc. Natl. Acad. Sci.* **111,** 16490–16495 (2014).
10. Mercier, P. P., Lysaght, A. C., Bandyopadhyay, S., Chandrakasan, A. P. & Stankovic, K. M. Energy extraction from the biologic battery in the inner ear. *Nat Biotech* **30,** 1240–1243 (2012).
11. Jung, W. *et al.* An Ultra-Low Power Fully Integrated Energy Harvester Based on Self-Oscillating Switched-Capacitor Voltage Doubler. IEEE J. Solid-State Circuits **49,** 2800–2811 (2014).
12. El-Damak, D. & Chandrakasan, A. P. A 10 nW-1 uW Power Management IC With Integrated Battery Management and Self-Startup for Energy Harvesting Applications. *IEEE J. Solid-State Circuits 51, 943–954 (2016).*
13. Zhang, S. *et al.* A pH-responsive supramolecular polymer gel as an enteric elastomer for use in gastric devices. *Nat. Mater.* **14,** 1065–1071 (2015).
14. Yin, L. *et al.* Materials, Designs, and Operational Characteristics for Fully Biodegradable Primary Batteries. *Adv. Mater.* **26,** 3879–3884 (2014).
15. Lee, K. B. & Lin, L. Electrolyte-based on-demand and disposable microbattery. *IEEE J. Microelectromechanical Syst.* **12,** 840–847 (2003).
16. Garay, E. F. & Bashirullah, R. Biofluid Activated Microbattery for Disposable Microsystems. *IEEE J. Microelectromechanical Syst.* **24,** 70–79 (2015).
17. Kim, Y. J., Chun, S.-E., Whitacre, J. & Bettinger, C. J. Self-deployable current sources fabricated from edible materials. *J. Mater. Chem. B* **1,** 3781–3788 (2013).
18. Hafezi, H. *et al.* An Ingestible Sensor for Measuring Medication Adherence. *Biomed. Eng. IEEE Trans. Biomedical Engineering* **62,** 99–109 (2015).
19. Jimbo, H. & Miki, N. Gastric-fluid-utilizing micro battery for micro medical devices . *Sensors Actuators B Chem.* **134,** 219–224 (2008).
20. Mostafalu, P. & Sonkusale, S. Flexible and transparent gastric battery: Energy harvesting from

gastric acid for endoscopy application . *Biosens. Bioelectron.* **54,** 292–296 (2014).
21. Di Maio, S. & Carrier, R. L. Gastrointestinal contents in fasted state and post-lipid ingestion: In vivo measurements and in vitro models for studying oral drug delivery. *J. Control. Release* **151,** 110–122 (2011).
22. Roy, O. Z. & Wehnert, R. W. Improvements in biogalvanic energy sources. *Med. Biol. Eng.* **12,** 50–56 (1974).
23. She, D., Tsang, M., Kim, J. K. & Allen, M. G. Immobilized electrolyte biodegradable batteries for implantable MEMS. in *Solid-State Sensors, Actuators and Microsystems (TRANSDUCERS), 2015 Transducers - 2015 18th International Conference on* 494–497 (2015).
24. *Dietary Reference Intakes for Vitamin A, K, Aresenic, Boron, Chromium, Copper, Iodine, Iron, Manganese, Molybdenum, Nickel, Silicon, Vanadium, and Zinc*. (Food and Nutrition Board, Institute of Medicine, USA, 2001).
25. Haynes, W. M. *CRC Handbook of Chemistry and Physics*. (CRC Press, 2015).
26. Kear, G., Barker, B. D. & Walsh, F. C. Electrochemical corrosion of unalloyed copper in chloride media—a critical review. *Corros. Sci.* **46,** 109–135 (2004).
27. *Datasheet. Low voltage digitially controlled potentiometer, ISL23315*. (Intersil, 2015).
28. *Datasheet. 8-Bit Flash Microcontroller with XLP Technology, PIC12LF1840T39A*. (Microchip, 2014).
29. Snoeck, V. *et al.* Gastrointestinal transit time of nondisintegrating radio-opaque pellets in suckling and recently weaned piglets. *J. Control. Release* **94,** 143–153 (2004).
30. Hossain, M., Abramowitz, W., Watrous, B. J., Szpunar, G. J. & Ayres, J. W. Gastrointestinal Transit of Nondisintegrating, Nonerodible Oral Dosage Forms in Pigs. *Pharm. Res.* **7,** 1163–1166
31. Traverso, G. *et al.* Microneedles for Drug Delivery via the Gastrointestinal Tract. *J. Pharm. Sci.* **104,** 362–367 (2015).
32. *Datasheet. Ultra Low Power Boost Converter with Battery Management for Energy Harverster Applications, BQ25504*. (Texas Instruments, 2015).
33. Santini, J. T., Cima, M. J. & Langer, R. A controlled-release microchip. *Nature* **397,** 335–338 (1999).
34. Santini Jr, J., Richards, A. C., Scheidt, R., Cima, M. J. & Langer, R. Microchips as Controlled Drug-Delivery Devices. *Angew. Chem. Int. Ed. Engl.* **39,** 2396–2407 (2000).
35. Singeap, A.-M. Capsule endoscopy: The road ahead. *World J. Gastroenterol.* **22,** 369 (2016).
36. Reardon, S. Electroceuticals spark interest. *Nature* **511,** 18 (2014).
37. Traverso, G. & Langer, R. Perspective: Special delivery for the gut. *Nature* **519,** S19–S19 (2015).
38. Niven, D. J. *et al.* Accuracy of peripheral thermometers for estimating temperature: a systematic review and meta-analysis. *Ann. Intern. Med.* **163,** 768–777 (2015).
39. Harpe, P., Gao, H., Dommele, R. v, Cantatore, E. & Roermund, A. H. M. van. A 0.20 3 nW Signal Acquisition IC for Miniature Sensor Nodes in 65 nm CMOS. *IEEE J. Solid-State Circuits* **51,** 240–248 (2016).
40. Yaul, F. M. & Chandrakasan, A. P. A 10 bit SAR ADC With Data-Dependent Energy Reduction Using LSB-First Successive Approximation. *IEEE J. Solid-State Circuits* **49,** 2825–2834 (2014).
41. Paidimarri, A., Ickes, N. & Chandrakasan, A. P. A +10dBm 2.4GHz transmitter with sub-400pW leakage and 43.7% system efficiency. in *IEEE ISSCC Dig. Tech. Papers* 1–3 (2015). doi:10.1109/ISSCC.2015.7063018
42. Fojtik, M. *et al.* A Millimeter-Scale Energy-Autonomous Sensor System With Stacked Battery

and Solar Cells. *IEEE. J. Solid-State Circuits* **48,** 801–813 (2013).
43. Kethu, S. R. *et al.* Endoluminal bariatric techniques. *Gastrointest. Endosc.* **76,** 1–7 (2012).
44. Rapoport, B. I., Kedzierski, J. T. & Sarpeshkar, R. A Glucose Fuel Cell for Implantable Brain-Machine Interfaces. *PLoS One* **7,** e38436–e38436 (2012).
45. Schoellhammer, C. M. *et al.* Ultrasound-mediated gastrointestinal drug delivery. *Sci. Transl. Med.* **7,** 310ra168-310ra168 (2015).
46. Nadeau, P. *et al.* Data for Prolonged energy harvesting for ingestible devices. (2017). Available at: http://dx.doi.org/10.6084/m9.figshare.4451420.

Acknowledgements

We thank J. Haupt, M. Jamiel and A. Hayward for help with the in vivo porcine work. We also thank A. Paidimarri for helpful discussions. A.P.C. was funded by Texas Instruments, the Semiconductor Research Corporation's Center of Excellence for Energy Efficient Electronics, and the Hong Kong Innovation and Technology Commission. R.L. was funded by a National Institutes of Health grant, EB-000244; a Max Planck Research Award, Ltr Dtd. 2/11/08; and the Alexander von Humboldt- Stiftung Foundation. G.T. was funded in part by the Division of Gastroenterology, Brigham and Women's Hospital.

Author Contributions

PN, DE-D, DG, YLK, NR, RL, AC, GT conceived and designed the research. PN, DE-D, SM, YLK, NR constructed prototypes for testing. PN, DE-D, DG, YLK conducted in vitro characterization. PN wrote the software for the capsules and offline processing the packets. PN, DE-D, DG, YLK, CC, LB, GT performed in vivo pig experiments. PN, DE-D, DG, YLK, NR, RL, AC, GT analyzed the data and wrote the manuscript.

Competing Interests

The authors declare that provisional patent application no. 62/328,084, covering a portion of this work, has been filed with the USPTO on April 27, 2016.

Figure captions

Figure 1 | Initial *in vivo* characterization and anode comparison. (a) Mg-Cu electrodes for probing the available power *in vivo* in different areas of the stomach and duodenum, with results shown in b, c and d. **(b)** Example of measured electrode voltage and output power density versus load current density (2 mm x 2 mm electrodes, duodenum). **(c)** Measured peak power density (horizontal bars denote mean), taken at the peak indicated in b, for different electrode sizes and locations (N = 3). **(d)** Voltage at peak power in c (N = 3), **(e)** Electrode configuration for anode comparison *in vitro* with measurements given in f and g. **(f)** Measured peak power density across time for both anode configurations. **(g)** Summary of the measured performance.

Figure 2 | Electrical characterization of the gastric battery in a porcine model. (a) Simplified architecture of the measurement system. **(b)** Photograph of the front and reverse sides of the system along with encapsulation using epoxy and PDMS. The PCB includes the programmable load resistor (DCP), crystal (XTAL), microcontroller (μP), RF matching network (MATCH), and antenna (ANT) on the front side, and the battery (BATT) and decoupling capacitor (CAP) on the reverse. **(c)** Diagram of the experimental setup, including photograph of the encapsulated pill in contact with gastric fluid inside the porcine stomach. **(d, e, f)** *In vivo* power characterization for a representative device (C4) including d: the voltage at the point of maximum power extraction during each sweep frame, e: the peak extracted power level in each frame and f: the measured body temperature. **(g)** X-rays at two time points showing passage from the stomach to the small intestine and the corresponding drop in observed power. **(h)** Statistical summary of the source voltage characterization data for 8 deployed

devices (window size, 1h; IQR, interquartile range). **(i)** Corresponding peak power measurements for the 8 devices.

Figure 3 | Demonstration of the gastric cell powering temperature measurement, wireless transmission, and drug delivery. **(a)** Architecture of the harvesting system. **(b)** The fabricated and encapsulated system printed circuit board. **(c)** Snapshot of storage capacitor during continuous harvesting in SGF. **(d)** Summary of the *in vivo* measured performance of three deployed devices in a porcine model. (electrode area: 30 mm x 3 mm, thickness: 2 × 250μm). **(e)** Example of the full *in vivo* measurement data for a representative device (D1), including the estimated average power harvested by the board in t = 1 h windows versus time and the overall average power (red line). **(f)** *In vivo* measurement of the body temperature performed using the harvested power. **(g)** Received signal strength indication (RSSI) at the receiver for packets transmitted from the body using the harvested power. **(h)** Image of a drug release prototype device, placed on a United States dime (scale bar, 5 mm). **(i)** Cross-sectional view of the device in h, where methylene blue is contained in a PMMA reservoir sealed with a 300 nm gold membrane and epoxy. **(j)** Demonstration of self-powered release (blue tail) from the device (yellow box) after activation in a beaker of porcine gastric fluid. Inset shows sequential images where the simulated drug is released in gastric fluid through gold corrosion. The gold membrane is intact in the beginning (t = 5 min) before triggered corrosion weakens the gold membrane causing crack formation on the film at t = 155 min (as shown by blue arrows), and ultimately the release of significant amount of methylene blue as shown at 355 min (blue color dye, shown in the red arrow). **(k)** Electrical profile during delivery of a pulse of charge to the release electrode. The dark line is the storage capacitor voltage and the lighter line is the voltage on the gold release electrode.

Figure 1

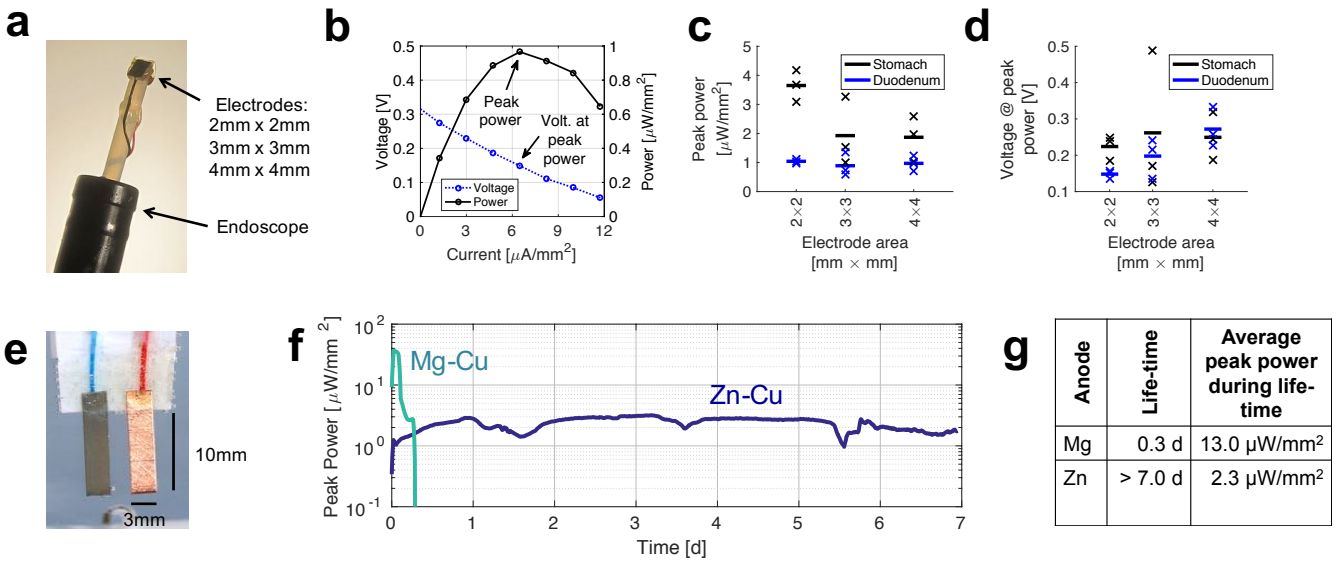

g

Anode	Life-time	Average peak power during life-time
Mg	0.3 d	13.0 μW/mm²
Zn	> 7.0 d	2.3 μW/mm²

Figure 2

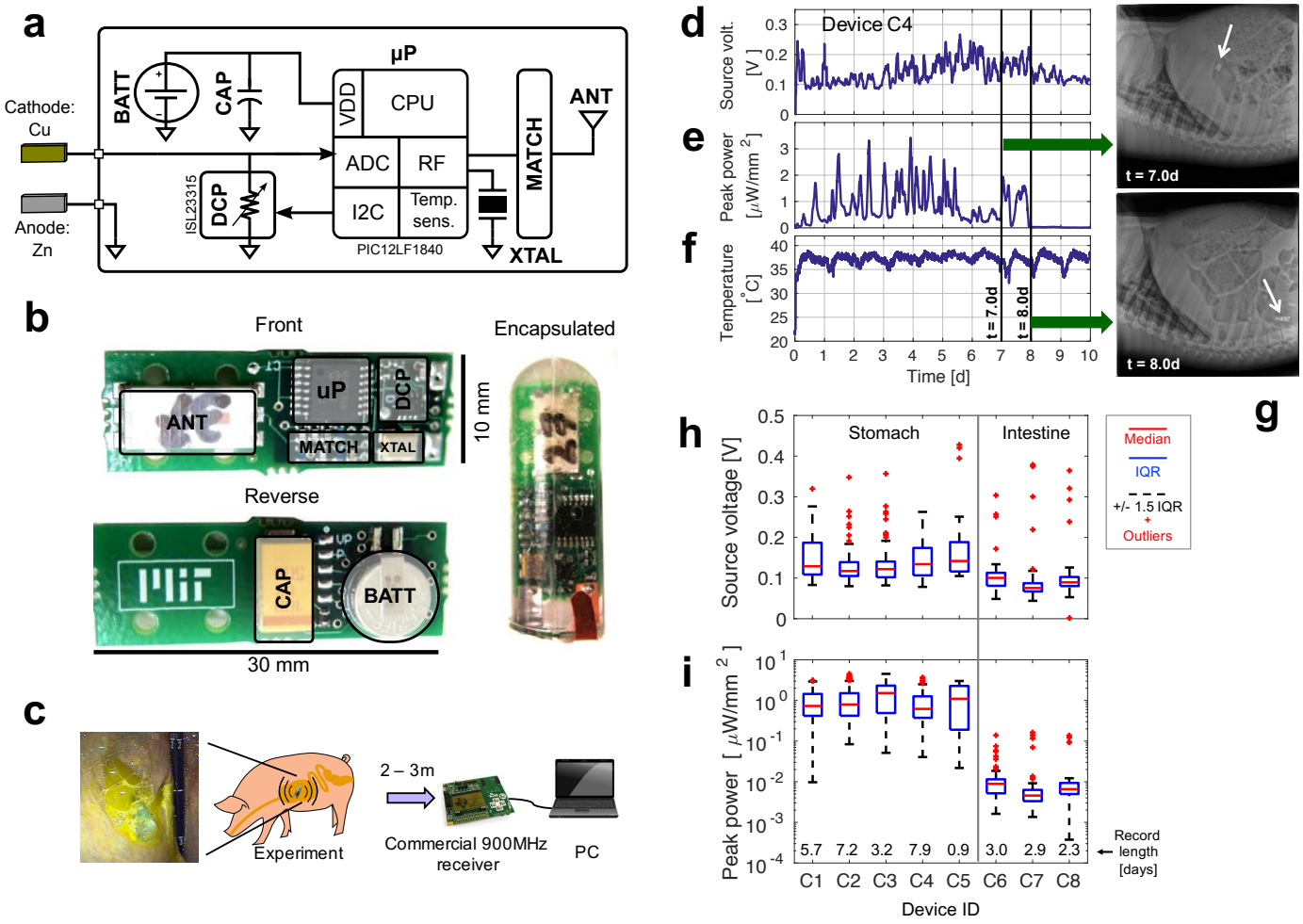
a
Cathode: Cu
Anode: Zn
BATT
CAP
ISL23315
DCP
μP
VDD
CPU
ADC
RF
I2C
Temp. sens.
PIC12LF1840
MATCH
ANT
XTAL
b
Front
Encapsulated
ANT
uP
DCP
MATCH
XTAL
10 mm
Reverse
CAP
BATT
30 mm
c
Experiment
2 – 3m
Commercial 900MHz receiver
PC
d
Device C4
Source volt. [V]
e
Peak power [μW/mm 2]
f
Temperature [°C]
t = 7.0d
t = 8.0d
Time [d]
g
t = 7.0d
t = 8.0d
h
Stomach
Intestine
Source voltage [V]
Median
IQR
+/- 1.5 IQR
Outliers
i
Peak power [μW/mm 2]
5.7 7.2 3.2 7.9 0.9 3.0 2.9 2.3
Record length [days]
C1 C2 C3 C4 C5 C6 C7 C8
Device ID

Figure 3

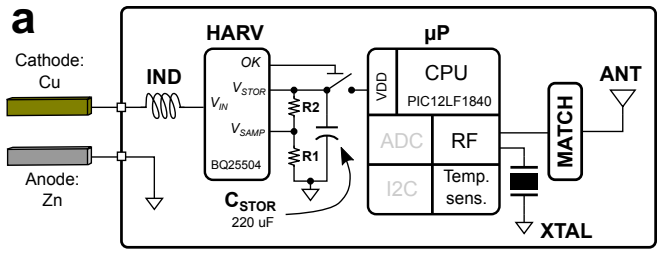

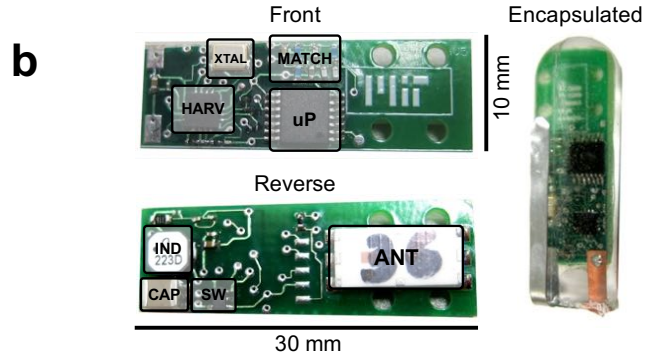

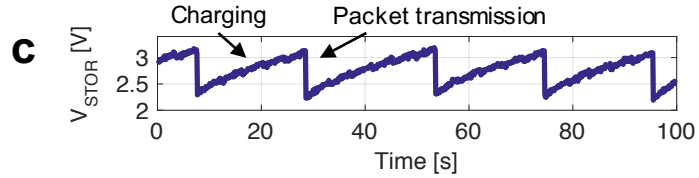

d

Dev.	Time	Average			Total energy density
		Packet interval	Power delivered	Power density	
	[d]	[s]	[uW]	[uW /mm^2]	[mJ/ mm^3]
D1	6.82	15.7	13.6	0.151	177
D2	6.61	14.0	16.0	0.178	203
D3	4.73	6.8	32.0	0.356	292

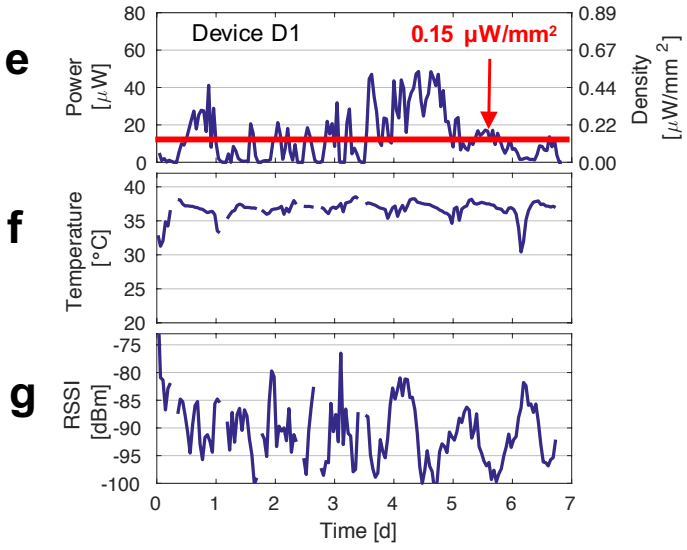

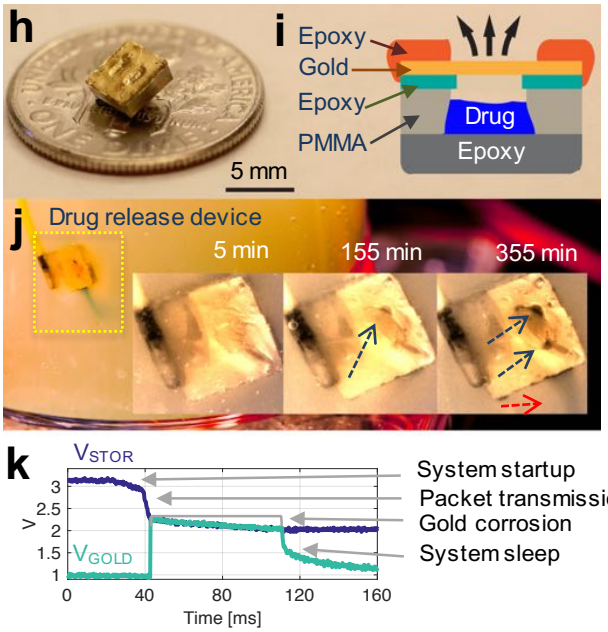

Supplementary Information for

Prolonged energy harvesting for ingestible devices

Authors

Phillip Nadeau[1], Dina El-Damak[1], Dean Glettig[2], Yong Lin Kong[2], Stacy Mo[2], Cody Cleveland[2,3], Lucas Booth[2], Niclas Roxhed[2,4], Robert Langer[2,5,6,*], Anantha P. Chandrakasan[1,*], Giovanni Traverso[2,3,*]

Affiliations

[1] Department of Electrical Engineering and Computer Science, and the Microsystems Technology Laboratories, Massachusetts Institute of Technology, Cambridge, Massachusetts 02139, USA

[2] Department of Chemical Engineering and Koch Institute for Integrative Cancer Research, Massachusetts Institute of Technology, Cambridge, Massachusetts 02139, USA.

[3] Division of Gastroenterology, Brigham and Women's Hospital, Harvard Medical School, Boston, MA 02115

[4] Department of Micro and Nanosystems, KTH Royal Institute of Technology, 10044 Stockholm, Sweden

[5] Media Lab, Massachusetts Institute of Technology, Cambridge, Massachusetts 02139, USA

[6] Institute for Medical Engineering and Science, Massachusetts Institute of Technology, Cambridge, Massachusetts 02139, USA

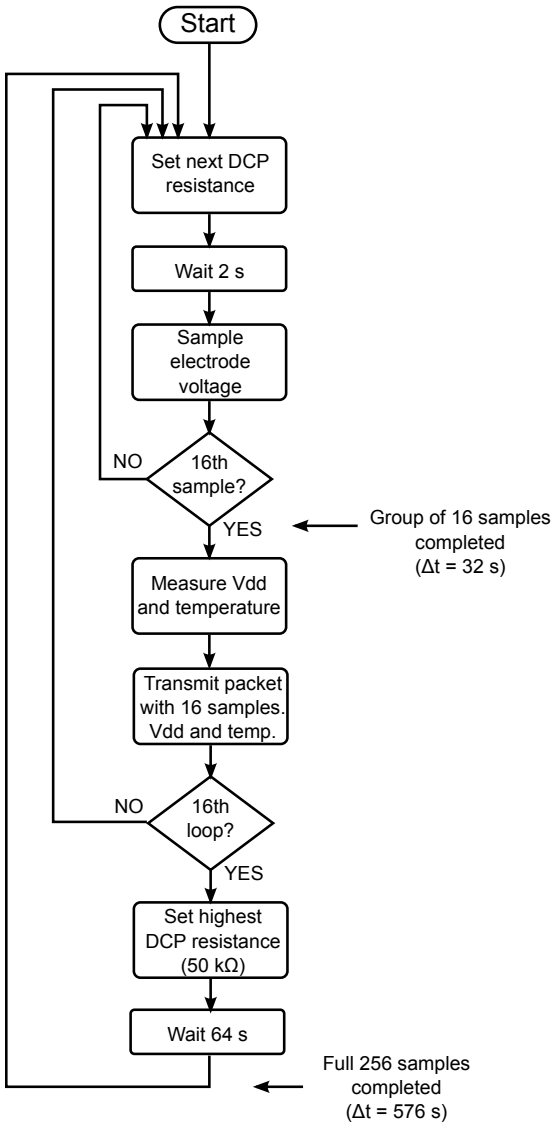

Supplementary Figure 1: Flow diagram for the measurement micro-code used for the resistance sweep.

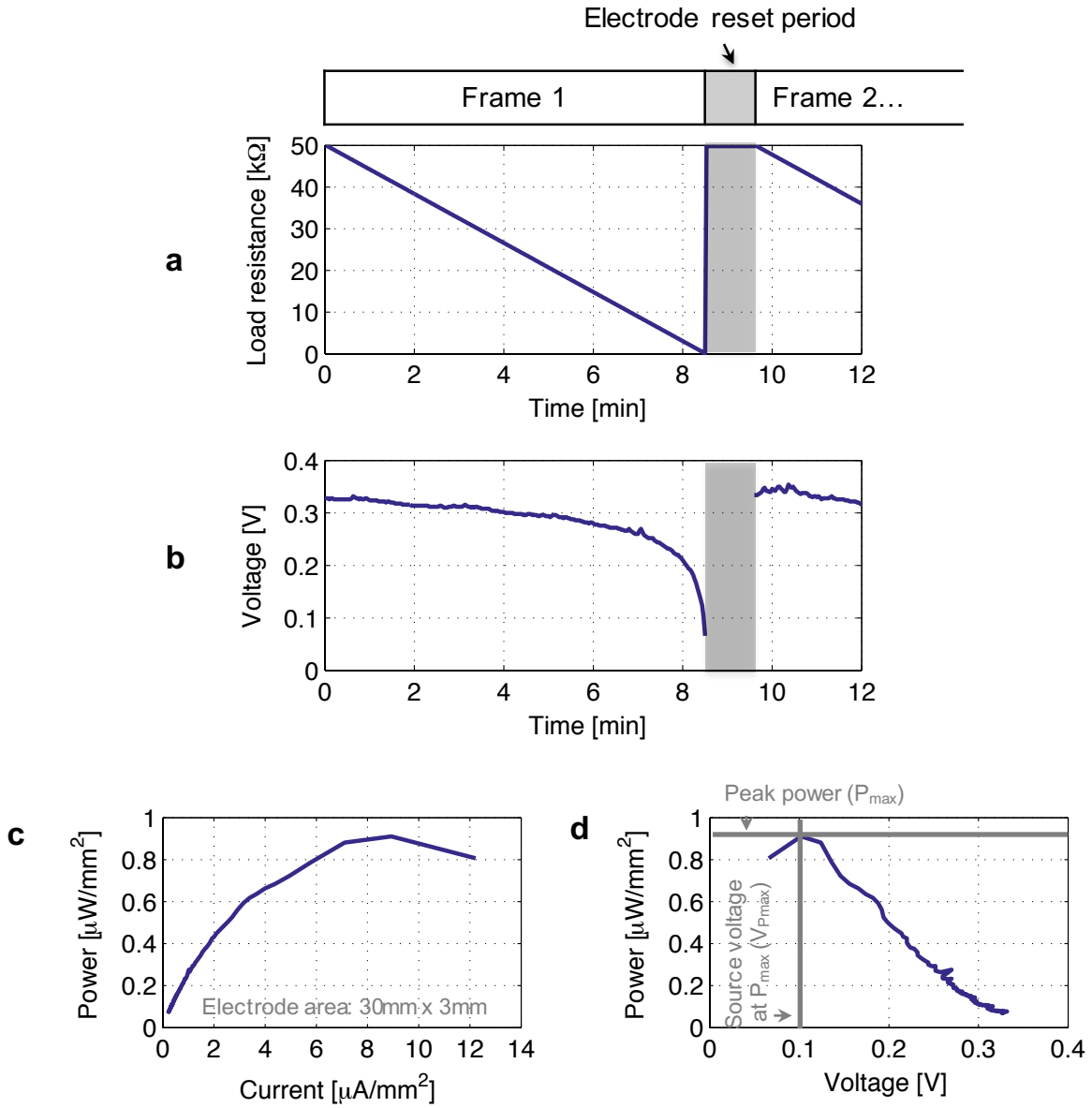

Supplementary Figure 2: Example *in vivo* characterization waveforms using the load sweep. (a) Sweep of the load resistance. **(b)** Measured voltage across the electrodes for the load resistance supplied in (a). **(c)** Measured power density versus current density, calculated from the first frame of (a) and (b). **(d)** Measured power density versus electrode voltage calculated from the first frame of (a) and (b).

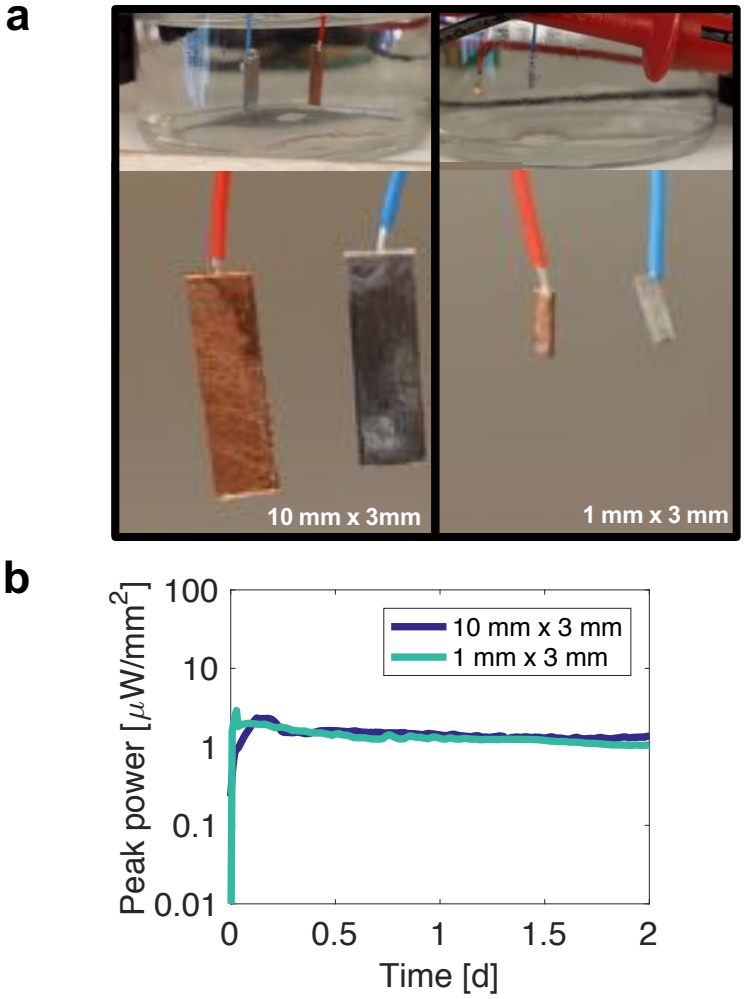

Supplementary Figure 3: Peak power characterization of two electrode areas (Zn-Cu, 30 mm^2, and 3 mm^2) in SGF. (a) Photo of the electrode setup and the electrodes. The wire connections are insulated with epoxy prior to the submersion in the SGF. (b) Measured power density across 48h.

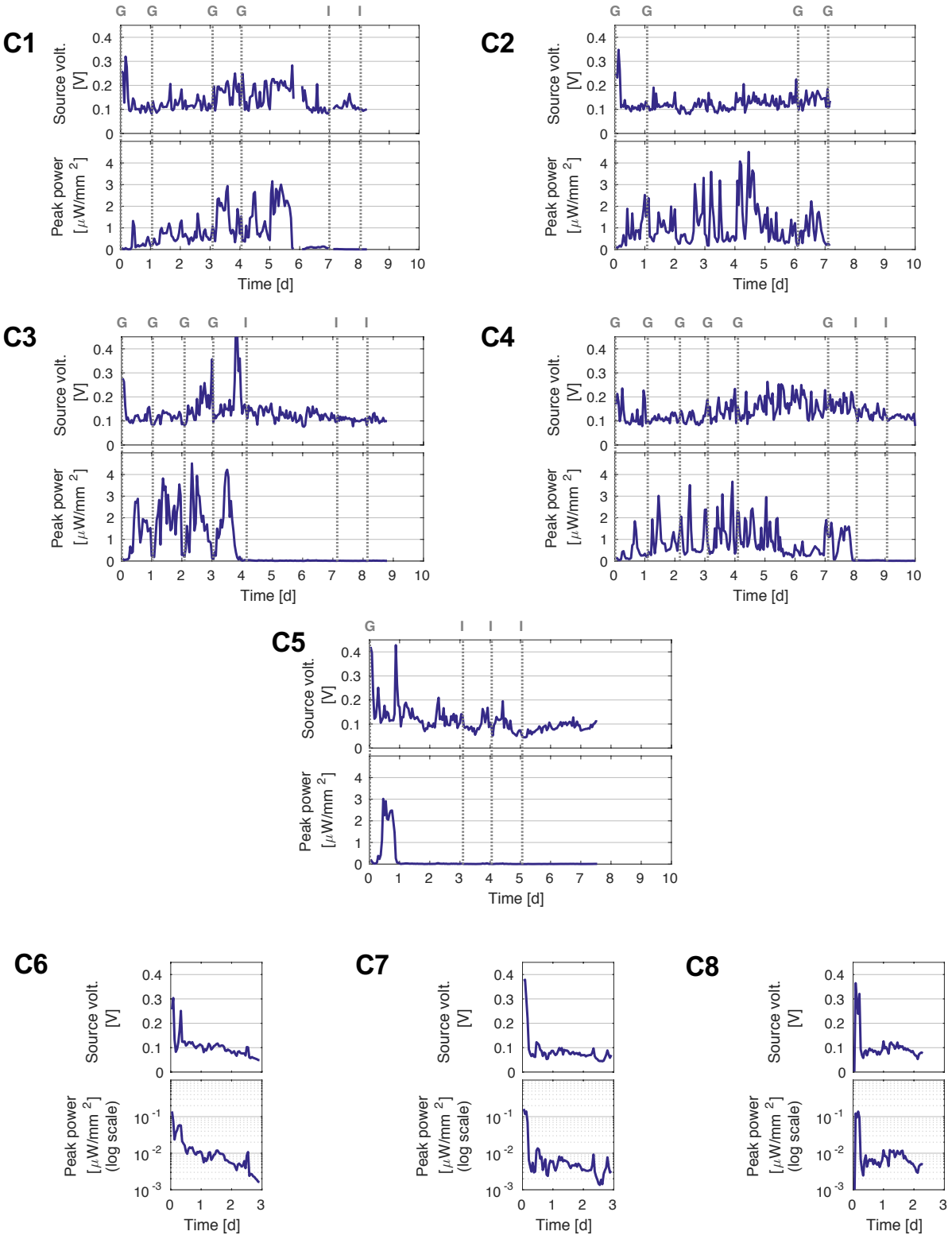

Supplementary Figure 4: Measured peak power density (P_{max}) and source voltage (obtained at the peak power, V_{Pmax}) for five capsules deposited in the stomach (C1 to C5) and three capsules deposited in the small intestine (C6 to C8). The sampling rate is one sample every 576 s, and the data are averaged into bins of size 1 h for display. The dashed lines in C1 to C5 indicate the times at which x-rays were taken: 'G' indicates when the capsule was determined to be in the gastric cavity and 'I' indicates the capsule was in the intestine.

Device	Deposit Location	Electrode Length	Time[1] (T)	Average during T	
				Volt. at Peak Power	Peak Power
		(w = 3mm)			[μW/mm²]
C1	Stomach	30 mm	5.71 d	0.148 V	0.98
C2	Stomach	10 mm	7.16 d	0.127 V	1.07
C3	Stomach	10 mm	3.20 d	0.135 V	1.58
C4	Stomach	10 mm	7.86 d	0.144 V	0.88
C5	Stomach	10 mm	0.88 d	0.185 V	1.21
C6	Small Int.	10 mm	3.01 d	0.102 V	0.0138
C7	Small Int.	10 mm	2.90 d	0.090 V	0.0121
C8	Small Int.	10 mm	2.27 d	0.101 V	0.0136

1 *(C1,C3,C4,C5)* Time of passage to the small intestine, estimated as the duration after which the measured peak power level remained below 0.20 μW/mm².

(C2) Device malfunctioned before passage to the intestine. The total available measurement duration of 7.16 d is used.

(C6, C7, C8) Total measurement duration until the capsule exited the body.

Supplementary Figure 5: Summary of power and voltage levels measured with the characterization capsule in a porcine model.

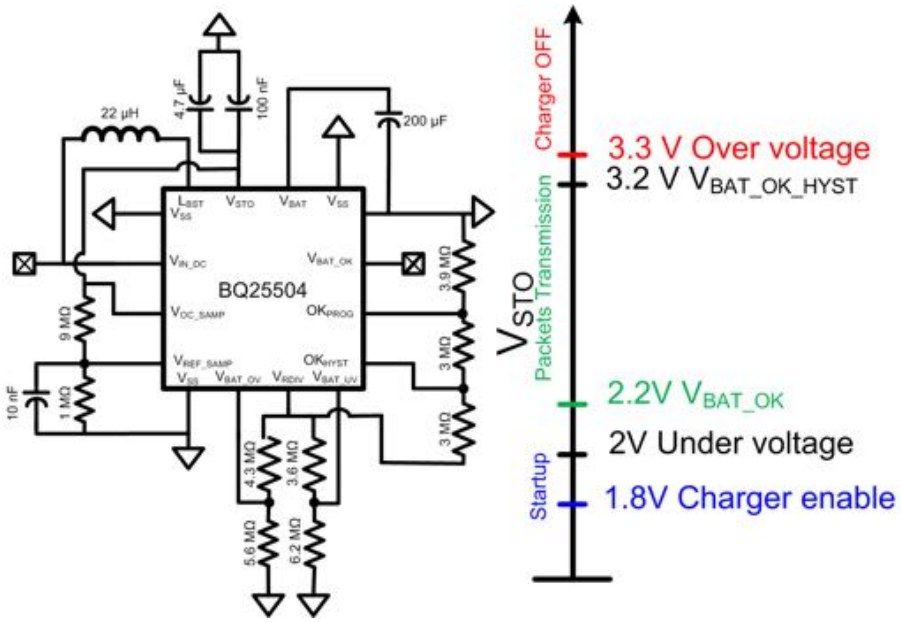

Supplementary Figure 6: Connection diagram for the energy harvesting boost-converter IC. The voltage on the storage capacitor is regulated to 3.3 V, and after startup, the voltage at the input is regulated to a fixed ratio of the storage capacitor voltage (1/12th). The OK signal turns on and starts the microcontroller code once the storage capacitor reaches 3.2 V, and turns off if the voltage declines to below 2.2 V.

a

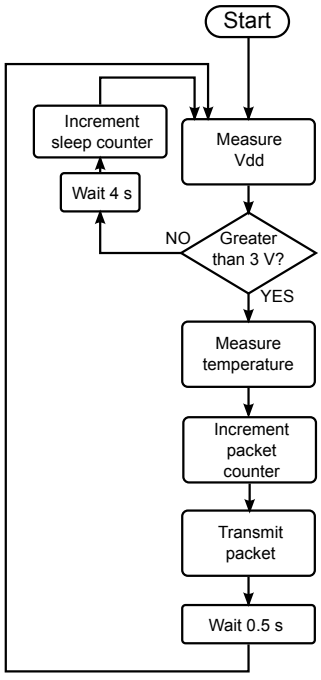

b

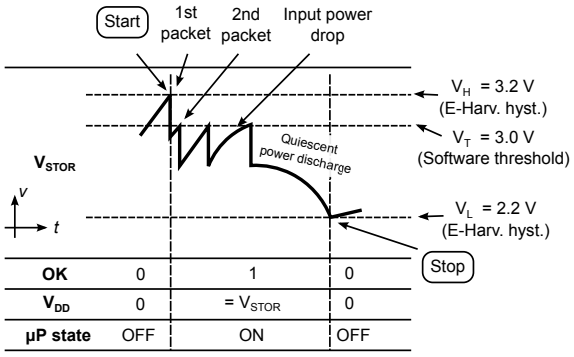

c

Vdd	Packet energy
3.0	196.5 µJ
3.1	207.7 µJ
3.2	217.6 µJ
3.3	229.4 µJ

Supplementary Figure 7: Energy harvesting demonstration setup. **(a)** Flow diagram for the microcontroller code. **(b)** Illustration of the starting and stopping of the microcontroller code based on the storage voltage relative the to the hysteresis levels set by the energy harvesting IC. (c) Measured energy consumption for a packet versus storage voltage level.

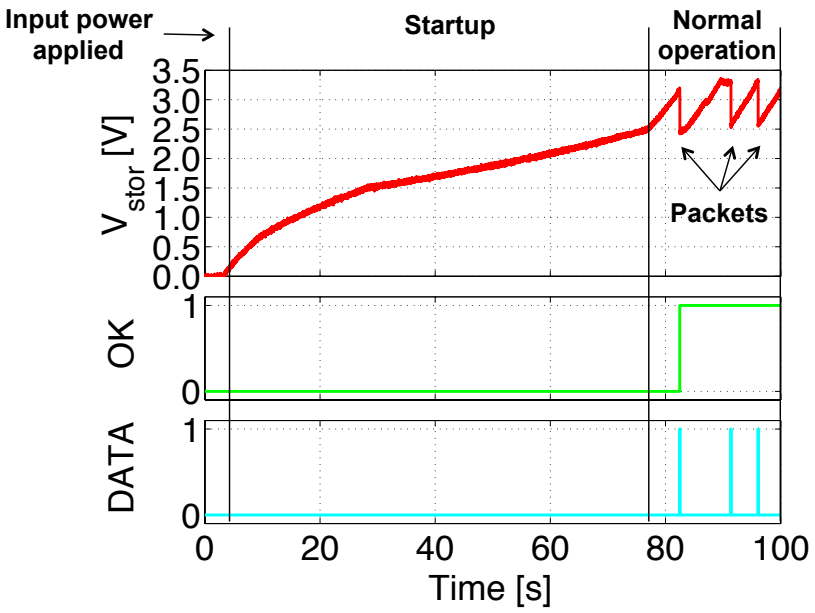

Supplementary Figure 8: Measured waveforms during bench-top operation (I_{in} = 400 µA). The top red trace is the voltage across the storage capacitor. The middle green trace is a digital signal that is low during the startup and ensures the microcontroller remains disconnected from the storage capacitor. The bottom cyan trace is the transmitted data.

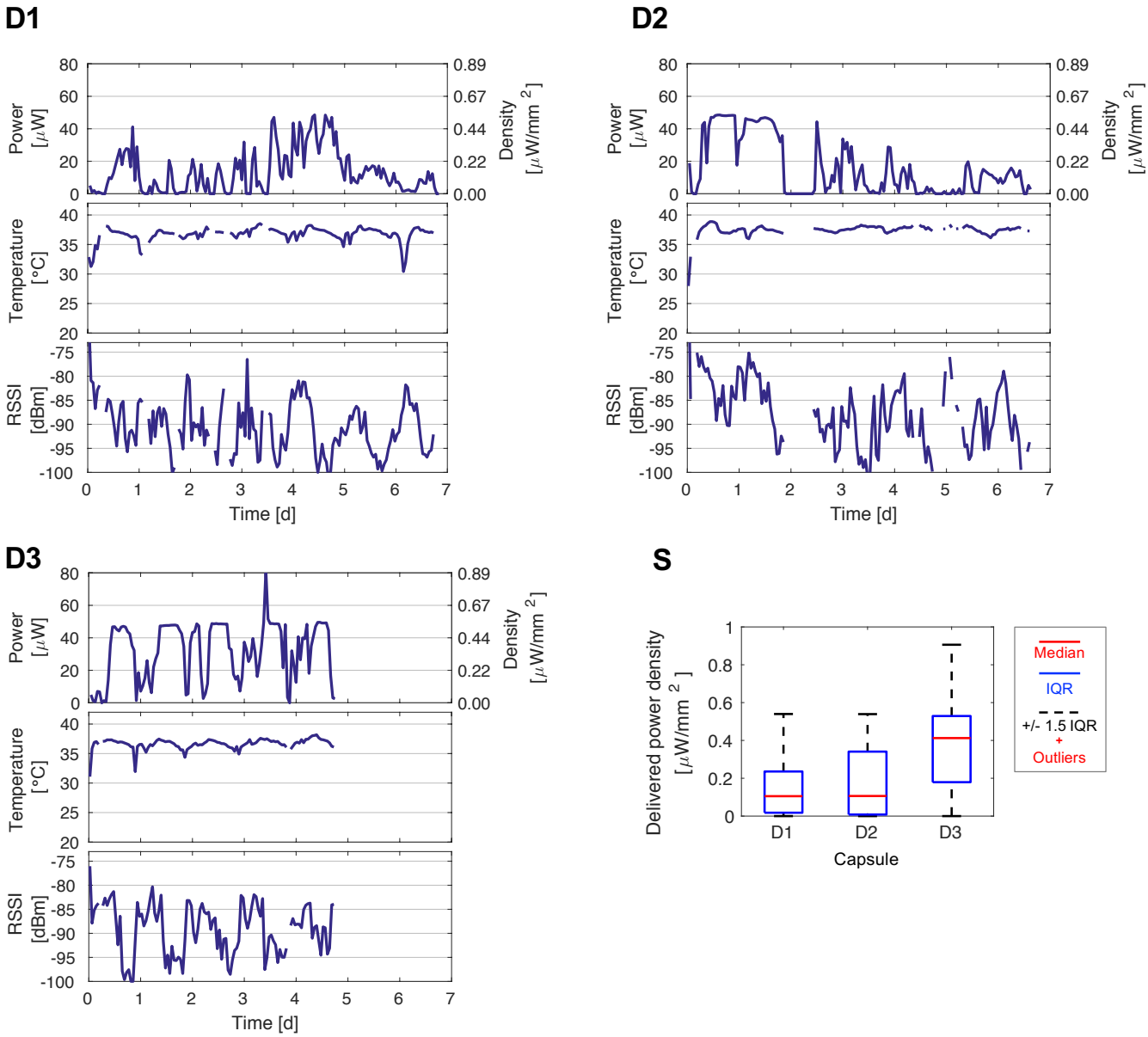

Supplementary Figure 9: Measurements from three harvesting capsules (D1 to D3) deposited in the stomach of a porcine model. Top plot: average power delivered to the system load, estimated using the number of transmitted packets. Middle plot: temperature measurement result. Bottom plot: RF signal strength at the receiver basestation. All data are captured at the variable arrival rate of the packets (every 12s on average across all three experiments) and averaged into bins of size t = 1 h for display. **(s)** Statistical summary of the power availability.